Available online at www.sciencedirect.com
ScienceDirect
Scripta Materialia 57 (2007) 877–880
Scripta MATERIALIA
www.elsevier.com/locate/scriptamat

An enriched continuum model for the design of a hierarchical composite

Shailendra P. Joshi* and K.T. Ramesh

Department of Mechanical Engineering, The Johns Hopkins University, Baltimore, MD 21218, USA

Received 17 May 2007; revised 11 June 2007; accepted 20 June 2007
Available online 3 August 2007

Hierarchical composites comprise two or more constituent phases where at least one phase is itself a composite at a finer scale. We present a multiscale secant Mori–Tanaka method incorporating length scale effects to describe the composite response. The applicability of the model is illustrated for the Al-based composite developed by Ye et al. [Scripta Materialia 53 (2005) 481], which exhibits impressive strength and some ductility. This rapid analytical approach enables numerical experiments that yield optimal composite architecture to be performed.

Keywords: Hierarchical microstructures; Particulate-reinforced composites (MMC); Mechanical behavior; Micromechanical modeling; Secant Mori–Tanaka approach

The quest for lightweight structural materials that possess high strength has led to the development of materials with heterogeneous microstructures [1]. Particularly in metals, secondary phases may be introduced in the form of dispersoids and precipitates for strengthening; ceramic or other non-metallic particulates (or fibers) may also be embedded, yielding metal–matrix composites (MMCs) with matrix-inclusion topologies [2]. In addition to the reinforcing effect due to the load transfer mechanism, experimental studies on these materials indicate that the composite strengthening depends inversely on the particulate size for a given volume fraction [2,3]. Recent advances in nanostructured materials have provided new impetus for designing even stronger composite materials [4–7], exploiting the interplay between the deformation mechanisms active at different length scales [8]. In such nanostructured composites, classical continuum approaches must be augmented with length scale dependent terms within the constitutive framework e.g. through the geometrical dislocation density (GND) argument [9] and gradient plasticity theories [10].

In this paper, we cast these approaches within a larger framework, that of hierarchical composites (Fig. 1). In this framework, a level-I composite is integrated with an additional phase to form a level-II composite (which can be integrated further to a level-III composite, and so on). This hierarchical concept is motivated by both properties and processing drivers. From a mechanical properties viewpoint, size effects and reinforcement can be used to derive materials with unusually high strengths, but the requirement of acceptable ductility necessitates the development of a level-II composite. From a processing viewpoint, each level of a hierarchical composite may represent the output of a different processing step. For example, the processing route required to generate and control the length scales associated with high strength may not be able to generate a fully dense material (or it may be difficult to retain macroscopic spatial control of microstructure and microscopic length scale simultaneously).

We note that nature tends to design hierarchical composites (e.g. abalone shells), using growth mechanisms (nature's equivalent of processing) to develop the levels of hierarchy while retaining very fine length scale control [11]. Our long-term research objective is to provide a conceptual basis for the design of artificial hierarchical composites. We focus here on elastoplastic behavior, leaving fracture response for a subsequent work.

For elastoplastic response, our approach is based on the secant Mori–Tanaka (sM–T) method [12,13] to describe the overall response of hierarchical composites with each of many phases deforming elastoplastically. The "trimodal" Al-composite discussed by Ye et al. [4] is used as an example to illustrate the utility of this

* Corresponding author. Tel.: +1 410 516 5162; fax: +1 410 516 7254; e-mail: spjoshi@jhu.edu

1359-6462/$ - see front matter
doi:10.1016/j.scriptamat.2007.06.061

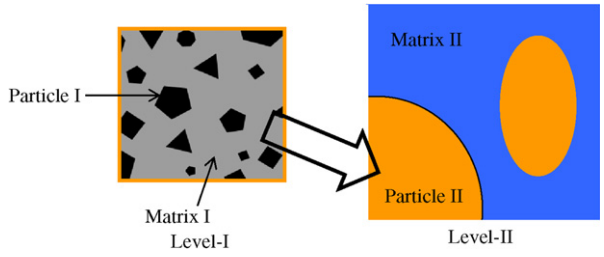

Figure 1. A schematic showing the hierarchical modeling concept.

approach. The choice of this lightweight composite as a model material is motivated by its characteristic microstructure and the resulting remarkable strength (~1 GPa) under both quasi-static [4] and dynamic conditions [7]. In addition to the direct strengthening through the load transfer between the ceramic and the matrix, our model includes so-called "non-continuum effects" due to several important length scales prevalent in the material, i.e. grain size, particulate reinforcement size and dispersoid spacing. The model is developed through an approach that closely follows the processing routes used in the fabrication of the composite. The essence of the approach is shown in Figure 1, with the M–T approach used to obtain the effective response of the level-I composite, which is then used as input into the sM–T analysis of the level-II composite. Non-continuum effects are accounted for in the level-I analysis since all of the major length scales are subscale to level-I.

As an example of this approach, consider the trimodal Al-based composite described by Ye et al. [4]. The microstructure of this unusually strong and light material is shown in Figure 2 at two scales: optical microscopy (Fig. 2a) and transmission electron microscopy (Fig. 2b). At the larger scale, we observe bright regions of micrograined 5083 aluminum (Al_{MG}) interdispersed with darker regions. At the fine scale (Fig. 2b), the dark regions of Figure 2a are seen to contain ultrafine-grained 5083 aluminum (Al_{UFG}) flecked with B_4C particles.

This characteristic microstructure arises directly from the two-stage processing route [4,5]. In stage I, 80 wt.% of Al-5083 (Al_{UFG}) powder and 20 wt.% B_4C particles are blended and then cryomilled. In stage-II, unmilled MG-Al5083 (Al_{MG}) is added to 50 wt.% of the cryomilled product of stage I processing, and this is followed by consolidation and hot extrusion resulting in the final "10–40–50" (10% B_4C–40% Al_{UFG}–50% Al_{MG}) composite called trimodal-Al by Ye et al. [4].

Given this microstructure, the analysis occurs at two levels, representing the hierarchical nature of the material (Fig. 1): the level-I composite is essentially that of Figure 2b, with Al_{UFG} containing particulate elastic (B_4C) inclusions, and the level-II composite corresponds to the integration of the level-I and MG components in Figure 2a.

The level-I constitutive response is obtained using the classical M–T approach for elastic inclusions embedded in an elastoplastic matrix. However, there are several subscale strengthening mechanisms that must be incorporated to account for size effects. These include: (i) the Hall–Petch effect due to grain size refinement, (ii) the GNDs arising from the thermoelastic mismatch between particles and matrix, (iii) the Orowan mechanism due to dispersoids that are distributed in the matrix by the cryomilling, and (iv) prior plastic work done by cryomilling and extrusion. This level-I analysis explicitly accounts for these subscale mechanisms. The level-II analysis then takes the level-I response as input and includes the response of the MG phase, resulting in the overall (composite) material response.

We first develop the subscale terms necessary for the level-I analysis, and then present the M–T analysis for the level-I composite.

1. Grain size strengthening. For an average grain size (d_g) of the cryomilled Al_{UFG} of 165–200 nm and the Hall–Petch coefficient (k_y) as 0.28 MPa $m^{1/2}$ [14], the strengthening ($\Delta\sigma_g = k_y d_g^{-1/2}$) due to grain size is 690–625 MPa.

2. Particle size strengthening. The GND densities due to mismatch in the elastic moduli and coefficients of thermal expansion (CTEs) between Al matrix and B_4C particles are [15]:

$$\rho_{GND}^{EM} = \frac{6 f_r \varepsilon}{b d_r}, \quad \rho_{GND}^{CTE} = \frac{12 f_r \varepsilon}{b d_r}, \tag{1}$$

where d_r the average particle size, f_r the particle volume fraction in the level-I composite, $\varepsilon(=\Delta\alpha\Delta T)$ the imposed strain during thermomechanical consolidation, $\Delta\alpha$ the CTE mismatch, ΔT the difference between the processing temperature and room temperature, and b the magnitude of the Burgers vector. The matrix strength increments due to the GND densities are [15]:

$$\Delta\sigma_{GND}^{EM} = \sqrt{3}\eta\mu_m b\sqrt{\rho_{GND}^{EM}}, \quad \Delta\sigma_{GND}^{EM} = \sqrt{3}\beta\mu_m b\sqrt{\rho_{GND}^{CTE}}, \tag{2}$$

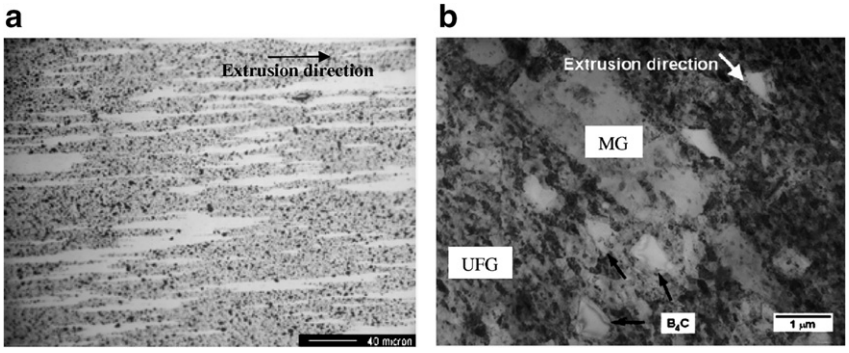

Figure 2. (a) Optical micrograph and (b) TEM image of a 10–40–50 composite.

where μ_m(=27 GPa) the shear modulus of the matrix, and $\eta = 0.5$ and $\beta = 0.7$ are the geometric constants. The thermomechanical treatment for the composite involves extrusion at a temperature of 525 °C, resulting in $\Delta\sigma_{GND}^{EM} = 45$ MPa and $\Delta\sigma_{GND}^{CTE} = 155$ MPa.

3. Dispersoid strengthening. Nanoscale dispersoids ($d_d = 10$ nm)are formed in the UFG phase during cryomilling. This results in Orowan strengthening [4]:

$$\Delta\sigma_{OR} = M\frac{0.4\mu_m b}{\pi(1-\upsilon)^{1/2}}\frac{ln(cd_d/b)}{\lambda}, \quad (3)$$

where M the Taylor factor, υ the matrix Poisson's ratio, λ the dispersoid spacing (deduced from TEM observations), and c gives an effective dispersoid diameter. From Eq. (3) we obtain a strength increment range of 55–130 MPa.

Traditionally these individual strengthening contributions are superposed either linearly or quadratically [16]. The different conventional superposition approaches give us less than 10% difference in the strength and so we choose the simple linear superposition scheme. The strength of the Al_{UFG} matrix phase in the level-I composite becomes

$$(\sigma_I)_{ufg} = \sigma_0 + \Delta\sigma_g + \Delta\sigma_{GND}^{CTE} + \Delta\sigma_{GND}^{EM} + \Delta\sigma_{OR}, \quad (4)$$

where σ_0 the yield strength of conventional Al-5083 (130 MPa). Using the lower estimates of the contributions from the individual mechanisms (Eqs. (1)–(3)) in Eq. (4), we obtain a strength estimate of 1000 MPa for the Al_{UFG}.

The M–T approach requires full stress–strain curves for both the matrix and the inclusion phases [12]. The post-yield behavior of the matrix is assumed to be identical to the cryomilled Al-5083(AL_{UFG}) of similar grain size, which showed a brief strain-hardening region followed by saturation of the flow stress σ_s. We use the Voce equation to represent the behavior of this material since it captures the saturation response:

$$\frac{\sigma_s - \sigma}{\sigma_s - \sigma_y} = \exp\left(\frac{-\varepsilon_p}{\varepsilon_c}\right), \quad (5)$$

where σ_y the matrix yield strength, ε_p the macroscopic plastic strain, and σ_s and ε_c are the saturation stress and the characteristic strain obtained by fitting the experimental data. The Voce parameters for the matrix are: $\sigma_y = (\sigma_1)_{UFG} = 1000$ MPa (from Eq. (4)); $\sigma_s = 1130$ MPa and $\varepsilon_c = 0.0064$ [12]. The elastic properties of B_4C are: $E = 480$ GPa; $\upsilon = 0.17$ and its volume fraction (v.f.) is 20%. The M–T method then provides the overall response of the level-I composite, which we use as an input to the level-II analysis.

In our hierarchical model, we consider a matrix-inclusion topology in level-II analysis that comprises 50% v.f. of the level-I composite combined with 50% v.f. of Al_{MG} (based on stage-II of the processing).

First, we fit the Voce equation to the overall level-I response (the fitted parameters are: $\sigma_y|_I = 1220$ MPa; $\sigma_s|_I = 1440$ MPa; $\varepsilon_c|_I = 0.025$ with a calculated elastic modulus of 95.4 GPa). The behavior of the Al_{MG} phase in the level-II composite must now be determined. The grain size in the MG phase ranges from 800 to 1000 nm. The plastic strains from the extrusion are accommodated primarily by the MG phase rather than the much harder level-I composite. Considering the grain size $d_{MG} = 800$ nm and with $k_y = 0.15$ MPa $m^{1/2}$ for unmilled Al-5083 [14], the estimated yield strength after grain size refinement for this Al_{MG} is 360 MPa. The extrusion ratios used here correspond to a plastic strain of approximately 200%. The difference between the saturation stress (σ_s) and the initial yield stress (σ_y) of the extruded Al_{MG} is similar to that of Al_{UFG} (i.e. 130 MPa), so that the extrusion elevates the yield stress level to 490 MPa, with the subsequent saturation behavior same as that of Al_{UFG}.

Figure 3 shows a comparison of the computed overall responses (σ–ε) and the measured compressive response for the 10–40–50 composite (blue curve). The computed stress–strain responses are shown for two composite topologies. Case 1 (the red solid curve) is the overall response for the topology with the level-I composite ($Al_{UFG} + B_4C$) as the matrix phase and Al_{MG} as the inclusion phase, while case 2 (the green dashed curve) inverts the topology, so that the level-I composite is the inclusion. In both cases the predicted elastic modulus is about 82 GPa, which compares well with the measured elastic modulus of 83 GPa. Both responses show onset of non-linearity at around 545 MPa (indicating the yielding of the softer phase). However, the hardening response in the small strain (up to 2%) regime is softer for case 2 compared to case 1. In case 2, the soft matrix phase provides a weak constraint on the stiff inclusion phase. It is only at about 4% strain that the inclusion phase also starts deforming plastically and the overall response reaches saturation. On the other hand, for case 1 the stiffer phase ($Al_{UFG} + B_4C$) acts as the matrix and significantly constrains the plastically softer Al_{MG} phase (''microyielding''), resulting in an enhanced overall hardening up to about 2% strain. This latter behavior compares well with the experiment (rather than case 2) suggesting that even at a high volume fraction of the MG phase, the microstructure is such that the stiff phase acts as the matrix, providing enhanced hardening in the plastic flow.

Note that the experimental stress–strain curve does exhibit a softening response and failure (indicated by in Fig. 3), possibly due to the development of microcracks during loading. In the absence of damage and failure criteria, the model cannot predict such a behavior.

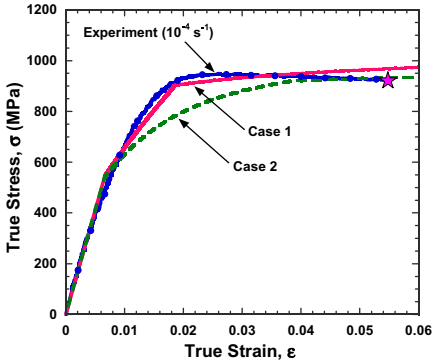

Figure 3. Comparison of the computed overall σ–ε responses with experimental results.

A key issue in the structural utility of nanostructured materials is the lack of ductility (the trimodal composite exhibits poor tensile ductility, <2%). One of the reasons for this is the lack of strain-hardening capacity in both the UFG and MG phases due to small grain sizes. Some important design questions for the trimodal material are:

1. What are the optimal particle and grain sizes and various volume fractions in the level-I composite?
2. What are the optimal grain sizes and volume fraction of the MG phase?

This highlights the possible degrees of freedom available in the design of this hierarchical composite. In this work, we do not seek solutions to the corresponding optimization problem. Instead, we perform numerical experiments using our model that can guide us toward obtaining an improved design. In particular, we focus on the interplay between the grain size contributions due to the UFG phase and the relatively coarser phase, keeping the particulate and the dispersoid parameters constant. With reference to our composite, the core strengthening is derived from the UFG structure (for a constant size and v.f. of the particulates and dispersoids). A simple strategy would be to achieve similar strengthening by reducing the average grain size of the UFG phase, and increasing the average grain size of the coarser phase. The idea is that the increased grain size of the coarse grained (CG) phase would impart higher strain-hardening and the corresponding reduction in the strength could be compensated by reducing the grain size of the UFG phase. In Figure 4 we compare three σ–ε responses: (A) baseline 10–40–50 composite response that compares with the experiments (same as case 1 in Figure 3); (B) a 10–40–50 composite response with a 100 nm size UFG phase (with 1 μm B_4C) and a CG phase (grain size > 10 μm; Voce parameters for CG Al-5083-H131 (curve 0, Fig. 4) are: $\sigma_y = 295$ MPa, $\sigma_s = 425$ MPa and $\varepsilon_c = 0.035$) (C) a 12–48–40 composite response with the same grain sizes as in case B. In all cases we employ the hierarchical analysis approach presented earlier.

The numerical experiments highlight several interesting features. Curve B shows the occurrence of microyielding (around 325 MPa) earlier than curve A. This is expected as the inclusion phase in B is plastically softer than that in A; however, the material response still exhibits the high constraining effect of the stiff matrix on the inclusions. The predicted Considerè ductility of B (blue circle) shows an increase of nearly 100% over that of the original composite (red circle) due to the strain-hardening capacity of the CG phase. The constraining effect (and correspondingly the microyielding) can be further enhanced by increasing the v.f. of the matrix phase (curve C, solid green line). As seen, increasing the matrix v.f. also increases the strength, while the ductility (green circle) remains comparable to curve B. Thus, these numerical experiments provide quick and useful insights into the possible design space for super strong and ductile lightweight composites.

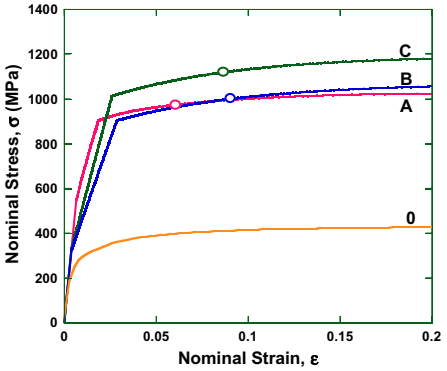

Figure 4. Computed overall σ–ε responses for different grain sizes in the UFG and the CG regimes. See text for discussion.

In summary, we have presented a multiscale secant Mori–Tanaka approach to simulate the mechanical behavior of hierarchical composites. Size-dependent strengthening mechanisms are also incorporated into the continuum response for a specific example, that of a trimodal composite material. For this model material the influence of matrix-inclusion topology on the overall response provides important guidelines in designing the microstructures of such composites. Our analysis indicates that the ductility could be enhanced by judiciously choosing pertinent length scales for the composite.

The authors thank Professor J.M. Schoenung (UC-Davis) for providing the micrographs in Figure 2. This work was performed under the auspices of the Center for Advanced Metallic and Ceramic Systems (CAMCS) at the Johns Hopkins University, supported by the Army Research Laboratory under the ARMAC-RTP Cooperative Agreement Nos. DAAD19-01-2-0003 and W911NF-06-2-0006.

[1] D.B. Miracle, Composites Science and Technology 65 (2005) 2526.
[2] D.J. Lloyd, International Materials Reviews 39 (1994) 1.
[3] M. Kouzeli, A. Mortensen, Acta Materialia 50 (2002) 39.
[4] J. Ye et al., Scripta Materialia 53 (2005) 481.
[5] J. Ye, J. He, J.M. Schoenung, Metallurgical and Materials Transactions A 37A (2006) 3099.
[6] J. Ye et al., Metallurgical and Materials Transactions A 37A (2006) 3111.
[7] H. Zhang et al., Advanced Engineering Materials 9 (2007) 355.
[8] A. Arzt, Acta Materialia 46 (1998) 5611.
[9] C.-W. Nan, D.R. Clarke, Acta Materialia 44 (1996) 3801.
[10] Z. Xue, Y. Huang, M. Li, Acta Materialia 50 (2002) 149.
[11] F. Barthelat, H. Tang, P.D. Zavattieri, C.-M. Li, H.D. Espinosa, Journal of the Mechanics and Physics of Solids 55 (2007) 306.
[12] S.P. Joshi, K.T. Ramesh, B.Q. Han, E.J. Lavernia, Metallurgical and Materials Transactions A 37 (2006) 2397.
[13] G.J. Weng, Journal of the Mechanics and Physics of Solids 38 (1990) 419.
[14] D. Witkin, E.J. Lavernia, Progress in Materials Science 51 (2005) 1.
[15] L.H. Dai, Z. Ling, Y.L. Bai, Composites Science and Technology 61 (2001) 1057.
[16] T.W. Clyne, P.J. Withers, An Introduction to Metal Matrix Composites, Cambridge University Press, Cambridge, 1993.